HTML ABSTRACT + LINKS

On the mechanical properties and phase behavior of silica: A simple model based on low coordination and strong association

Matthew H. Ford
Department of Chemical Engineering, University of Massachusetts, Amherst, Massachusetts 01003

Scott M. Auerbach
Department of Chemical Engineering, University of Massachusetts, Amherst, Massachusetts 01003 and Department of Chemistry, University of Massachusetts, Amherst, Massachusetts 01003

P. A. Monson[a)]
Department of Chemical Engineering, University of Massachusetts, Amherst, Massachusetts 01003

(Received 23 June 2004; accepted 2 August 2004)

We present a simple and computationally efficient classical atomistic model of silica in which the silicon and oxygen are simulated as hard spheres with four and two association sites, respectively. We have performed isobaric-isothermal Monte Carlo simulations to study the mechanical and phase behavior of this model. We have investigated solid phase structures of the model corresponding to quartz, cristobalite, and coesite, as well as some zeolite structures. For the model these phases are mechanically stable and highly incompressible. Ratios of zero-pressure bulk moduli and thermal expansion coefficients for α quartz, α cristobalite, and coesite are in quite good agreement with experimental values. The pressure-temperature phase diagram was constructed and shows three solid phases corresponding to cristobalite, quartz, and coesite, as well as a fluid or glass phase, behavior qualitatively similar to that seen for silica experimentally. © *2004 American Institute of Physics.* [DOI: 10.1063/1.1797979]

I. INTRODUCTION

Silica is one of the most versatile compounds in modern materials research, forming nanoporous zeolites,[1–4] photonic crystals,[5–7] and a variety of ordered and disordered adsorption materials.[8] Designing materials for advanced applications often requires a detailed understanding of structure and performance over several length scales, from angstroms to microns and beyond. An example of such hierarchical self-assembly is the synthesis of silicalite-1 (an ultralow aluminum MFI framework zeolite) from a clear solution of silica nanoparticles.[2,9–13] To date, atomistic modeling of such hierarchical self-assembly has remained challenging. In this paper, we propose a model for silica that is both physically realistic and computationally efficient.

Previous statistical mechanical models of silica have been shown to reproduce accurately the structures and physical properties of selected silica polymorphs.[14–18] Some of these models are able to capture the nontrivial physics of certain phases, such as the melting of β cristobalite to a higher density fluid state,[19] the pressure-induced amorphization of α quartz,[20] and the phase transformation dynamics between α cristobalite and β cristobalite.[21] Such models are quite computationally intensive and it is worthwhile to ask whether a simpler model can be formulated that can nevertheless capture the mechanical properties and phase behavior of the different polymorphs of silica. In the present work, we view silica as a material dominated by low coordination and strong association, inspired by previous models of hydrogen bonded fluids.[22,23] For computational efficiency, these interactions are implemented through hard-sphere repulsions and directional square-well attractions. By examining the mechanical and phase behavior of this Si+O model, we show that it is in good qualitative agreement with experimental data on the dense silica phases.

The remainder of this paper is organized as follows: Sec. II details the model that has been developed, the solid phases that are of interest in this study, and gives the details of the Monte Carlo simulations we have used to study the model, including the methodology used to calculate free energies. Section III reports our results including the calculation of the phase diagram and a comparison of the results with those for real silica. Section IV contains a summary of our findings and some concluding remarks.

II. MOLECULAR MODEL AND CALCULATION METHODS

A. Molecular model

Our overall goal is to include the key chemical and physical properties of silica, while keeping the model computationally tractable. The key chemistry and physics includes the strong silicon-oxygen bond, the tetrahedral coordination of the oxygen atoms about a given silicon atom, and strong short-ranged repulsion. A simple way to do this is to adapt ideas from models of short range association in hydrogen bonding fluids. An example of this is the primitive model of water (PMW),[23] which has been shown to qualitatively reproduce aspects of the solid-fluid phase behavior of water.[24]

a)Electronic mail: monson@ecs.umass.edu

 © 2004 American Institute of Physics

Downloaded 29 Oct 2004 to 128.119.82.70. Redistribution subject to AIP license or copyright, see http://jcp.aip.org/jcp/copyright.jsp

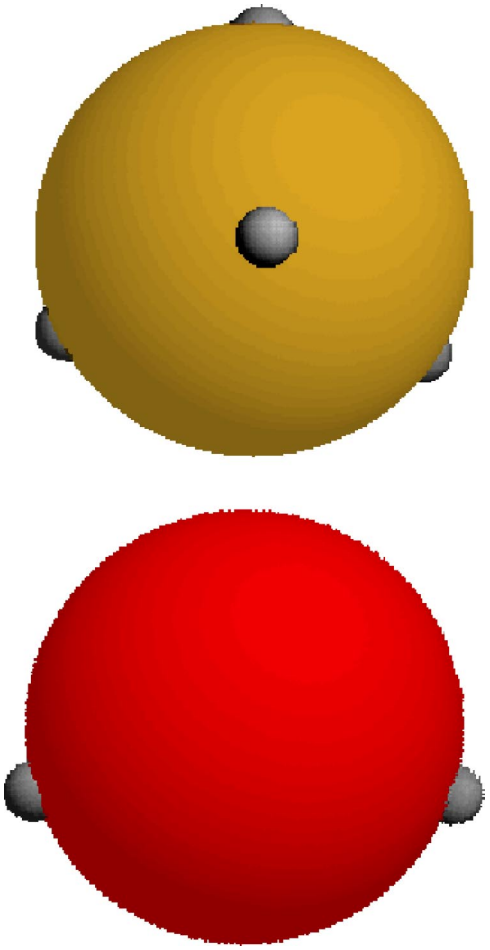

FIG. 1. A visualization of the molecular model of silica. Top: Representation of a silicon atom. Bottom: Representation of an oxygen atom. Similar to silicon it includes a hard core short range repulsion, but here there are only two bonding sites on the surface on the hard sphere. The angle formed by the two bonding sites is 145.8°, the average Si-O-Si angle exhibited in four low pressure phases of naturally occurring silica.

The present model represents silicon as a hard sphere core with four bonding sites tetrahedrally arranged on its surface (Fig. 1). This enforces the tetrahedral coordination of oxygen atoms about a single silicon atom. Oxygen is similarly described as a hard sphere with two bonding sites on its surface (Fig. 1). The placement of the bonding sites on oxygen is not as straightforward as that for silicon. The low pressure dense phases of silica have Si-O-Si angles that range between 140° and 150°, while in zeolitic frameworks the Si-O-Si bond angle can vary from as low as 130° to as high as 180°. We have chosen the angle between the bonding sites on oxygen to be 145.8°. This is the average of the Si-O-Si angles exhibited in α and β phases of quartz and cristobalite. Despite this constraint we show below that we can construct essentially all the phases of silica with four-coordinate silicon using this model.

The silicon-silicon and silicon-oxygen nonbonded interactions are hard sphere potentials with a hard sphere diameter σ. The oxygen-oxygen interaction is similar; however, it employs a nonadditive hard sphere interaction. The oxygen-oxygen interaction length is set to 1.6σ. This distance helps the model to reproduce the O-Si-O bond angle distribution predicted by molecular dynamics simulations.[15] The silicon-oxygen bonded interaction is modeled as

$$u_{\text{Si-O}}(r_{\text{Si-O}}) = \begin{cases} -\epsilon & r_{\text{Si-O}} \leqslant \lambda_w \\ 0 & r_{\text{Si-O}} > \lambda_w . \end{cases} \tag{2.1}$$

In order for the model to be robust, and simulate as many phases as possible, we wish to use the largest value of λ_w that will allow only one bond to form between any two bonding sites. We choose $\lambda_w = [1-(\sqrt{3}/2)]\sigma$ to preserve this stoichiometry.[23] This width also allows for Si-O-Si angles from $\approx 130°$ up to 180° to be simulated, allowing one simple model to simulate all phases of interest.

B. Solid phases studied

The solid phases considered in this study are, in the first instance, the naturally occurring phases: α quartz, β quartz, α cristobalite, β cristobalite, β tridymite, and coesite. The zeolite frameworks MFI (silicalite), SOD (sodalite), LTA (zeolite A), and FAU (faujasite) were also studied. The structures of α quartz, β quartz, α cristobalite, and β tridymite were obtained from the book of Wyckoff.[25] The β cristobalite structure reported in Wyckoff has too high a symmetry and is thought to represent an idealized crystal structure.[26–28] The β cristobalite structure used in this work was taken from Wright and Leadbetter,[26] and is a structure averaged over the dynamically disordered locations of the oxygen atoms. The structure of coesite was obtained from an atmospheric pressure refinement by Levien *et al.*[29] The high-pressure stishovite phase is not modeled due to the change in coordination chemistry of silica at high pressures. At pressures above 8–10 GPa the silicon coordination in silica goes from four-fold to sixfold. The assumed tetrahedral coordination of oxygen about silicon in our model prohibits the modeling of the $\text{Si}(\text{O}_6)_{1/2}$ base units of stishovite. Our solid phase simulations were initialized by placing the silicon and oxygen atoms at the fractional coordinates given in the experimentally determined crystal structures. To obtain the proper orientational configuration for each atom, a short Monte Carlo simulation was run using a single unit cell, allowing the atoms to rotate in their fixed lattice positions. Once the internal energy reached that of a fully bound crystal the simulation was ended and the final orientations were then used in the initial configuration for future simulations. All silica zeolite framework structures were obtained from the structural database of the International Zeolite Association.[30]

C. Monte Carlo simulations

Isobaric-isothermal (N-P-T) Monte Carlo (MC) simulation is the principal tool used for simulating the solid phase behavior of this model. Canonical Monte Carlo was also used in the simulation of the fluid phase. To allow for the noncubic unit cell shape of these phases, we used a method derived for molecular dynamics by Parrinello and Rahman[31] and adapted to Monte Carlo by others.[32,33] In this approach, the simulation box is not described by an edge length, but rather by a matrix consisting of the three vectors, each of which is an edge vector of the unit cell. The matrix is denoted by

Downloaded 29 Oct 2004 to 128.119.82.70. Redistribution subject to AIP license or copyright, see http://jcp.aip.org/jcp/copyright.jsp

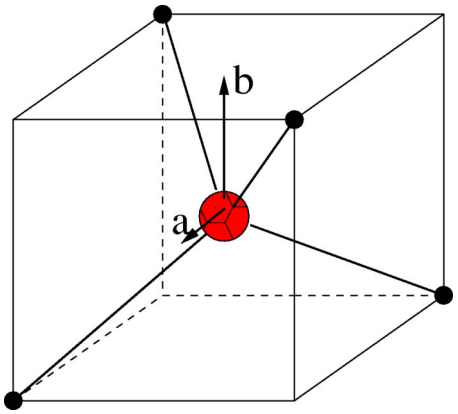

FIG. 2. Body-fixed vectors **a** and **b** used in the solid phase free energy calculations.

$$\mathbf{H}=[\underline{a}\,\underline{b}\,\underline{c}]. \tag{2.2}$$

This allows not only for noncubic box shapes, but for the shape of the simulation cell to change during the simulation run. The volume of the simulation cell is then defined as

$$V=\det(\mathbf{H}). \tag{2.3}$$

A typical simulation consisted of 250 000 cycles for equilibration and 250 000 cycles for obtaining average statistics. One cycle consisted of N_{particle} attempts to perform particle translation, particle rotation, or a volume shift of the simulation cell. Volume shifts were attempted 1% of the time, while the remaining move types were attempted with equal probability. The volume shifts allow for both isotropic scaling and for anisotropic volume moves. Anisotropic volume changes include changing the relative lengths of each side, or changing the cell shape entirely. The acceptance ratio for translation and rotation moves was kept near 40%, whereas the volume change ratio was held closer to 20%. The typical system size for each phase studied was between 200 and 300 atoms. This corresponds to 8 $(2\times2\times2)$ or 27 $(3\times3\times3)$ unit cells depending on the crystal symmetry used in the initial configuration.

D. Free energy calculations

1. Solid phase

To calculate the solid phase free energies, we implemented the Frenkel-Ladd methodology.[34] This method creates a thermodynamic path between the solid of interest and a classical Einstein crystal. The Einstein field used in this work is given by

$$U_{\text{Einstein}}=\sum_{i=1}^{N}\left[\frac{\lambda}{\sigma^2}(\mathbf{R_i}-\mathbf{R_i^{(0)}})^2+\lambda\left(\frac{\psi_{a,i}}{\pi}\right)^2+\lambda\left(\frac{\psi_{b,i}}{\pi}\right)^2\right]. \tag{2.4}$$

where λ is the coupling constant. $\mathbf{R_i}$ and $\mathbf{R_i^{(0)}}$ represent the location of atom i for the current configuration, and in the reference lattice configuration, respectively. The angles ψ_a and ψ_b are defined as follows. Let $\mathbf{a}_i^{(0)}$ and $\mathbf{b}_i^{(0)}$ be two perpendicular unit vectors in body fixed coordinates assigned to each atom in the reference lattice (vectors **a** and **b** are shown in Fig. 2). Vectors $\mathbf{a}_i$ and $\mathbf{b}_i$ are the same vectors in the current configuration. $\psi_{a,i}$ is the angle between $\mathbf{a}_i^{(0)}$ and $\mathbf{a}_i$, and $\psi_{b,i}$ is that between $\mathbf{b}_i^{(0)}$ and $\mathbf{b}_i$.

The free energy of the model solid can be related to that of an ideal Einstein crystal via

$$A=A_E+\Delta A_1+\Delta A_2+\Delta A_3, \tag{2.5}$$

where A_E is the free energy of the ideal Einstein crystal and ΔA_1 is the difference between the free energy of the ideal Einstein crystal and that of the Einstein crystal with interactions. ΔA_2 gives the difference in free energy between the solid of interest and that of an Einstein crystal with interactions and ΔA_3 is the difference in free energy between a system with an unconstrained center of mass and that of a system with a fixed center of mass.

The free energy of the ideal Einstein crystal is made up of translational and rotational contributions. Expressions for these have been derived elsewhere.[24,34,35] We use a slightly modified expression for the rotational portion of the free energy resulting from the orientation dependence of the energy in our reference Einstein crystal. The orientational contribution to the free energy of the reference noninteracting Einstein crystal is given by

$$\frac{A_{E,or}}{Nk_bT}=-\ln\left(\frac{1}{8\pi^2}\int_0^{\pi}\int_0^{2\pi}\int_0^{2\pi}\exp\left\{-\frac{\lambda}{k_bT}\left[\left(\frac{\psi_a}{\pi}\right)^2+\left(\frac{\psi_b}{\pi}\right)^2\right]\right\}\sin\alpha\,d\alpha\,d\phi\,d\gamma\right), \tag{2.6}$$

where α, ϕ, and γ are the three Euler angles defining the orientation of a molecule. By choosing the $\mathbf{a}^{(0)}$ vector as parallel to the body-fixed z axis, we can simplify Eq. (2.6) by replacing ψ_a with the Euler angle α. The angle ψ_b is, in general, a function of all three Euler angles, however, for large values of λ the only significant contribution to the integral arises when α is close to zero. When α is near zero, the angle ψ_b can be identified with the Euler angle γ. This leads to a simplified expression for the rotational contribution to the free energy of the Einstein crystal

$$\frac{A_{E,or}}{Nk_bT}=-\ln\left[\frac{1}{2\pi}\int_0^{\pi}\exp\left\{-\frac{\lambda}{k_bT}\left(\frac{\alpha}{\pi}\right)^2\right\}\times\sin\alpha\,d\alpha\int_0^{\pi}\exp\left\{-\frac{\lambda}{k_bT}\left(\frac{\gamma}{\pi}\right)^2\right\}d\gamma\right]. \tag{2.7}$$

ΔA_1 is given by

$$\frac{\Delta A_1}{Nk_BT}=-\frac{1}{N}\ln\left\langle\exp\left[-\frac{1}{k_bT}\sum_{i<j}u(i,j)\right]\right\rangle, \tag{2.8}$$

where the angle brackets denote a canonical ensemble average over configurations of the noninteracting Einstein crystal and $u(i,j)$ is the pair potential of the solid of interest. When

Downloaded 29 Oct 2004 to 128.119.82.70. Redistribution subject to AIP license or copyright, see http://jcp.aip.org/jcp/copyright.jsp

λ is very large the hard core interactions make only a very small contribution to ΔA_1 compared with the boding interactions. ΔA_2 is given by

$$\frac{\Delta A_2}{Nk_BT}=\frac{1}{N}\int_{\lambda_{\max}}^{0}\left\langle\sum_{i=1}^{N}\left[\left(\frac{\mathbf{R_i}-\mathbf{R_i^{(0)}}}{\sigma}\right)^2+\left(\frac{\psi_{a,i}}{\pi}\right)^2+\left(\frac{\psi_{b,i}}{\pi}\right)^2\right]\right\rangle_{\lambda}d\lambda. \tag{2.9}$$

The angle brackets again denote a canonical average over the interacting Einstein crystal with the subscript denoting the value of the coupling constant. ΔA_3 is given by[36]

$$\frac{\Delta A_3}{Nk_BT}=-\frac{1}{N}\ln(V/N). \tag{2.10}$$

Further details of this method as it is applied to nonspherical molecules can be found elsewhere.[24,35,37,38]

2. Simplification of thermodynamic property calculations for fully bonded solid phases

For a fully bonded state of the model, the internal energy per atom is given by $U/N=-4\epsilon/3$, independent of the density. This allows for a significant simplification when computing the solid phase free energy as was first shown for the PMW.[24] This is seen as follows. Starting with the Gibbs-Helmholtz equation

$$\left(\frac{\partial A/T}{\partial T}\right)_{V,N}=-\frac{U}{T^2}, \tag{2.11}$$

and taking a volume derivative we obtain

$$\left[\frac{\partial}{\partial V}\left(\frac{\partial A/T}{\partial T}\right)_{V,N}\right]_{T,N}=-\frac{1}{T^2}\left(\frac{\partial U}{\partial V}\right)_{T,N}. \tag{2.12}$$

Since U is independent of density for fully bonded states of the model the right-hand side of this expression is zero. Using the expression $P=-(\partial A/\partial V)_{T,N}$ it follows that

$$\left(\frac{\partial P/T}{\partial T}\right)_{V,N}=0, \tag{2.13}$$

so that we can write that for a given density

$$P(T)=P(T_0)\left(\frac{T}{T_0}\right). \tag{2.14}$$

Similarly we can use the Gibbs-Helmholtz equation to show that for a given density

$$A(T)=A(T_0)\left(\frac{T}{T_0}\right)+U(T_0)\left(1-\frac{T}{T_0}\right). \tag{2.15}$$

These expressions show that we need to only generate the free energy and pressure on one isotherm for each phase of interest. We can obtain isotherms at other temperatures, where the system remains fully bonded, by using Eqs. (2.14) and (2.15). A few short simulations must be run to determine the temperature range for which Eqs. (2.14) and (2.15) are valid. The range of temperature where the solid is fully bound depends on the pressure and the solid phase geometry. For higher pressures and denser structures the solid is fully bound over a wider range of temperatures. The assumption of full bonding was found to be valid for all solid states considered in our work.

3. Fluid phase

The fluid phase free energy is typically computed by relating the system of interest to an ideal gas. The configurational Helmholtz energy of an ideal gas can be written as

$$\frac{A^{\mathrm{IG}}}{Nk_BT}=\ln\rho-1. \tag{2.16}$$

The Helmholtz free energy can then be determined at any density using

$$\frac{A(\rho)}{N}=\frac{A(\rho_0)}{N}+\int_{\rho_0}^{\rho}\frac{P}{\rho^2}d\rho. \tag{2.17}$$

However, this method requires a reversible path between the state of interest at density ρ and a very low density ideal gas state. This can be achieved by compressing the system of interest at low pressure and density to a high pressure, high density system, and then subsequently expanding back to the low density, low pressure starting state in order to check that the states are reversible. In the case of our system we have encountered difficulty in equilibrating the fluid at low temperatures (typically for values of $T^*=k_BT/\epsilon$ less than about 0.12). This reflects the tendency for the system to form strongly bound amorphous networks at moderate and high fluid densities. We have investigated some methods of enhancing the sampling in the Monte Carlo simulations, including hyperparallel tempering in the N-P-T ensemble[39] and density-of-states Monte Carlo[40–42] but these did not significantly enhance the equilibration of the systems.

In order to obtain estimates of the low temperature fluid behavior we have studied the isochoric behavior of the model in the fluid phase. It was found that isochores of the internal energy versus temperature are reversible over large regions of temperature, including lower temperatures for which the N-P-T simulations are unable to fully equilibrate the system. Using thermodynamic integration of the Gibbs-Helmholtz equation, we use isochores of the internal energy to compute the change in Helmholtz free energy between two temperatures at a given density. At temperatures well above the melting point of the model, where the bond strength is not the dominant factor, we can successfully generate reversible isotherms between ideal gas and compressed states, and therefore compute the Helmholtz free energy at a given temperature for a range of densities (volumes). A reversible isotherm was generated at $T^*=0.2$, well above the melting temperature of the solid phases. The Helmholtz free energy was computed for this isotherm through thermodynamic integration from an ideal gas reference state. Nineteen densities between the ideal gas state and the density of coesite were then chosen. Isochores of the internal energy at these densities were computed by progressively heating the system to $T^*=0.20$, and slowly cooling it back down to a temperature of 0.06. Free energy differences were then computed by integrating on these isochores. By using all the

Downloaded 29 Oct 2004 to 128.119.82.70. Redistribution subject to AIP license or copyright, see http://jcp.aip.org/jcp/copyright.jsp

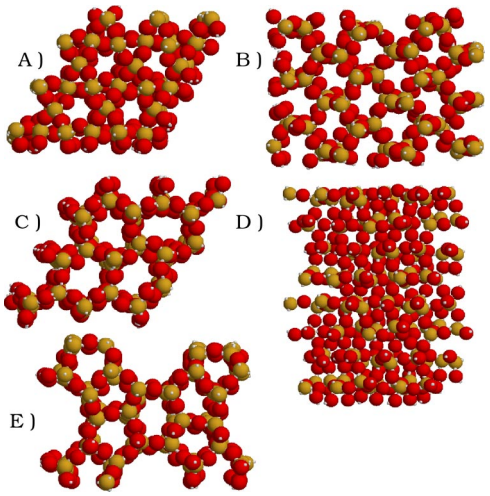

FIG. 3. Visualizations of equilibrated configurations taken from N-P-T Monte Carlo simulations at $P\sigma^3/\epsilon=0.00\,001$ and $kT/\epsilon=0.01$ initialized from different crystal structures of silica. (A.) α quartz structure taken from Wyckoff.[25] (B.) α cristobalite structure taken from Wyckoff[25] (C.) β tridymite structure taken from Wyckoff[25] (D.) Coesite structural data from atmospheric refinement by Levien[29] (E.) Silicalite-1 structure taken from van Koningsveld.[52]

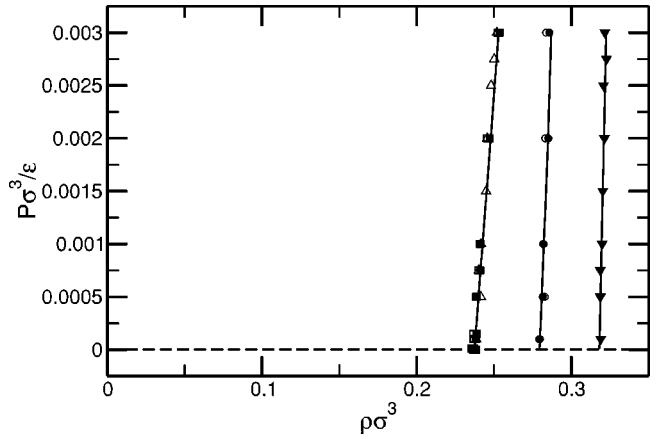

FIG. 4. Pressure ($P\sigma^3/\epsilon$) versus density ($\rho\sigma^3$) for the six different naturally occurring silica solid phases studied in this work. Solid lines are the equations of state in the form of Eq. (3.1) (○) α quartz, (●) β quartz, (□) α cristobalite, (■) β cristobalite, (△) β trydimite, and (▼) coesite.

information from each density, we constructed isotherms of the Helmholtz free energy, and used these to estimate the P-ρ behavior of the fluid.

III. RESULTS AND DISCUSSION

A. Mechanical behavior of Si+O model

We begin by exploring whether our model for silica is mechanically stable at finite pressures, and whether its mechanical properties are qualitatively correct. The phases of interest in this work are quartz, cristobalite, tridymite, and coesite. MFI, SOD, FAU, and LTA framework zeolite structures were also studied to determine if a very low density structure is also mechanically stable. One should note the wide variance in Si-O-Si bond angles exhibited in these crystal structures. Quartz and cristobalite both have a single Si-O-Si angle around 145°, MFI has 17 distinct bond angles ranging from 130° to 175°, while the idealized form of β tridymite has a 180° Si-O-Si angle. The finite square-well width for Si-O bonds allows this wide range of angles to occur within our model. Figure 3 shows snapshots of equilibrated structures generated by N-P-T Monte Carlo simulations of the model at low values of the pressure. It is evident that the overall coordination and crystal shape are preserved after equilibration. However, the small displacements of atoms result in some loss of the symmetry associated with respect to the input crystal structure.

Figure 4 is a plot of reduced pressure $P^*=P\sigma^3/\epsilon$ versus reduced density $\rho^*=\rho\sigma^3$ for each of the dense phases studied. These isotherms were generated from a sequence of N-P-T simulations where the final configuration from a simulation at pressure P_i was used as the initial configuration for the simulation at pressure P_{i+1}. This procedure was then reversed starting from the highest pressure, to check that the isotherms are thermodynamically reversible. It is evident that each phase examined is mechanically stable at a nonzero pressure. It should be noted that all of the square-well bonds are saturated at the temperature for which the isotherms were generated ($T^*=0.01$). Bond breaking is an extremely rare event for all temperatures below $k_BT/\epsilon\approx0.095$. Linear pressure-density equations of state (EOS) were fitted to the isotherms shown in Fig. 4 according to

$$P(\rho,T)=(A\rho+B)\left(\frac{T}{T_{\mathrm{ref}}}\right). \tag{3.1}$$

As noted above, this allows the $P\rho T$ behavior of the fully connected solid to be completely described using only this one isotherm. The order of densities provides an initial point of comparison between the model system and real silica. Our model predicts solid phase densities in the following order: cristobalite<quartz<coesite. Experimental data indicate that cristobalite has a solid density of 2.318 g/cm^3,[43] quartz a density of 2.646 g/cm^3,[44] and coesite that of 2.921 g/cm^3,[29] in qualitative agreement with our model. The steepness of the isotherms in Fig. 4 suggests a highly incompressible material. This is what one would expect for silica. In order to quantify the extent of incompressibility, we computed zero-pressure bulk modulus for each phase. The values obtained from the equations of state were checked by using fluctuation expressions in the N-P-T ensemble. Results for both methods were statistically equivalent. Table I shows the ratios of bulk moduli between pairs of solid phases computed from the present model and the corresponding ratios using experimental values. The good agreement between the model and experiment is a pleasing result given the model's simplicity. The model results reported in Table I are calculated from the equations of state for the solid phases. From this

TABLE I. Ratios of bulk moduli between different phases as computed in the model, compared to corresponding experimental ratios.

Phases	Simulation	Expt.[a]
Cristobalite/Quartz	0.45±0.07	0.44
Quartz/Coesite	0.47±0.10	0.40

[a]Reference 51.

Downloaded 29 Oct 2004 to 128.119.82.70. Redistribution subject to AIP license or copyright, see http://jcp.aip.org/jcp/copyright.jsp

TABLE II. Ratios of thermal expansion coefficients between two phases, compared with corresponding experimental ratios. Simulations were performed at a reduced pressure of zero. Experimental data are for expansion coefficients at 1 atm and 273 K.

Phases	Simulation	Expt.[a]
Cristobalite/Quartz	2.63±0.77	2.276
Quartz/Coesite	2.43±0.96	4.7

[a]Reference 51.

table we can see that in both experiment and in the model, the bulk modulus of cristobalite is the lowest, followed by quartz, and then coesite. To further test the model, thermal expansion coefficients were calculated from the equation of state [Eq. (3.1)] via

$$\alpha_P = \left(\frac{\partial V}{\partial T}\right)_P = -\left(\frac{\partial P}{\partial T}\right)_V \Big/ \left(\frac{\partial P}{\partial V}\right)_T . \tag{3.2}$$

Table II shows computed thermal expansion coefficient ratios for pairs of solid phases together with experimental values. Again, we can see that there is good agreement between the ratios except for the calculated quartz/coesite ratio. The amount of uncertainty in the experimental values is not precisely known. Overall, the data in Tables I and II indicate that our simple model captures the relative values of compressibilities and expansion coefficients among the different phases.

Given the wide range of angles reported in the crystal structures of different silica phases, it is interesting to compute the equilibrium distributions of angles that arise from our model. Figure 5 gives the distribution of bond angles generated from a low-pressure simulation of α quartz. The solid line is the O-Si-O bond angle distribution, while the dashed line is for Si-O-Si angles. There is a 13.5° full width at half maximum (FWHM) for the O-Si-O angle distribution, centered about 109°. From molecular dynamics simulations of amorphous silica, Vashishta *et al.*[15] reported a FWHM of 10° in the O-Si-O bond angle. We are unaware of data or calculations for the bond angle distribution for the crystalline phases. For the Si-O-Si bond angle, our simulations give a FWHM of 35° centered at 145°. Fitting ^{29}Si-NMR data of tridymite and amorphous SiO_2, Pettifer *et al.* reported a 30° variation in the Si-O-Si angle.[45] Simulations of other phases showed very similar behavior. However, the silicalite-1 phase shows a higher average Si-O-Si angle, but the width of the histogram is similar to that of α quartz.

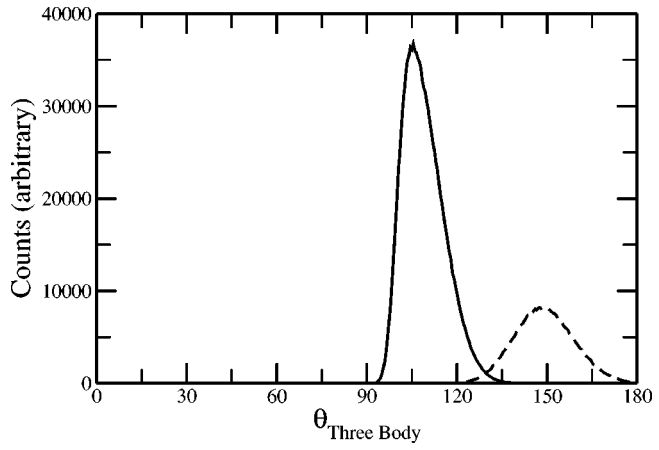

FIG. 5. Three-body angle distributions calculated for α quartz at reduced pressure $P\sigma^3/\epsilon = 0.0\,001$, and a reduced temperature of $k_BT/\epsilon = 0.01$. The solid line is the O-Si-O bond angle distribution centered at about 110°, the dashed line is the Si-O-Si angle distribution, centered at about 149°.

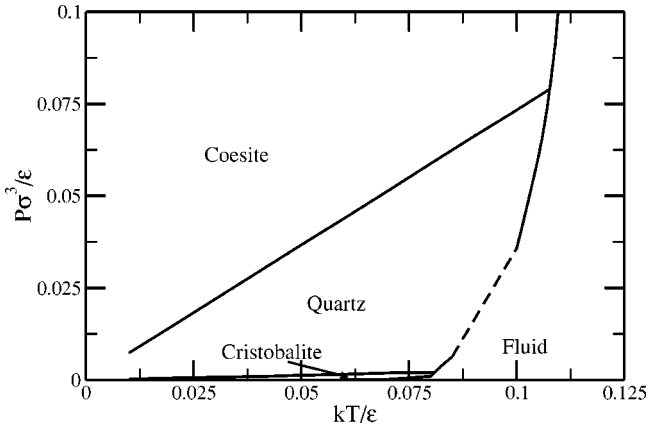

FIG. 6. Pressure ($P\sigma^3/\epsilon$) versus temperature (kT/ϵ) phase diagram. The dashed line denotes our estimate of the phase equilibrium for states where the fluid phase could not be equilibrated.

B. Phase behavior of Si+O model

Figure 6 shows the P^*-T^* phase diagram computed from our model of silica. The phase diagram shows the cristobalite-quartz and quartz-coesite solid-solid phase boundaries. A quartz-cristobalite-fluid triple point is found at $k_BT/\epsilon = 0.081$ and $P\sigma^3/\epsilon = 0.002$. A second triple point, among coesite, quartz, and the fluid is found at $k_BT/\epsilon = 0.107$ and a $P\sigma^3/\epsilon = 0.078$. When compared with the experimental pressure-temperature phase diagram (Fig. 7), it is evident that our model qualitatively describes the phase behavior of silica. In our model, the pressure dependence of the stable phase is properly captured, with cristobalite being stable at low pressures, quartz the stable phase at intermedi-

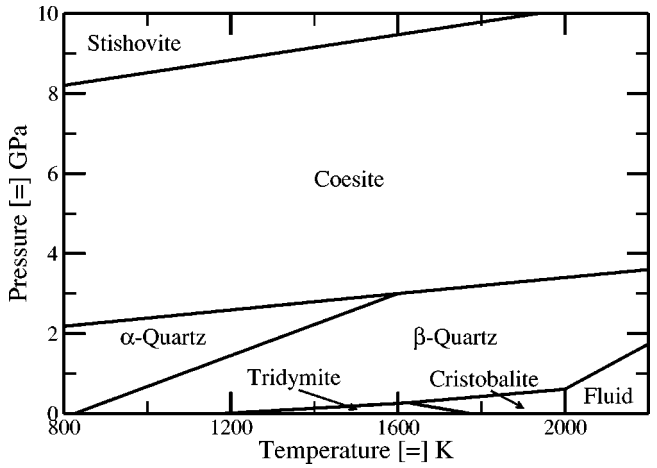

FIG. 7. Semischematic experimental pressure versus temperature phase diagram of silica. Based on data reported by Swamy[51] and references cited therein.

Downloaded 29 Oct 2004 to 128.119.82.70. Redistribution subject to AIP license or copyright, see http://jcp.aip.org/jcp/copyright.jsp

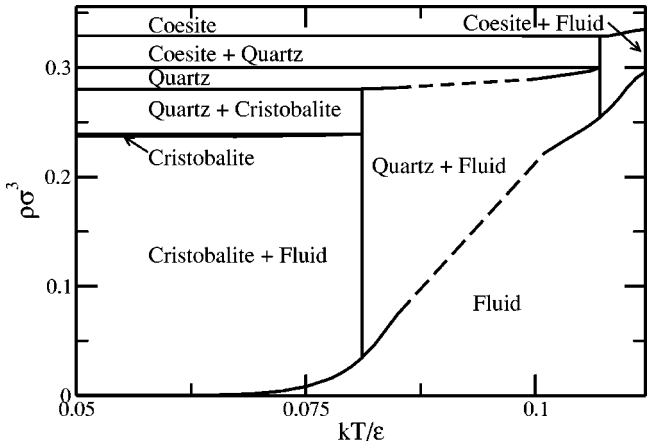

FIG. 8. Temperature (kT/ϵ) versus density ($\rho\sigma^3$) phase diagram for the model of silica.

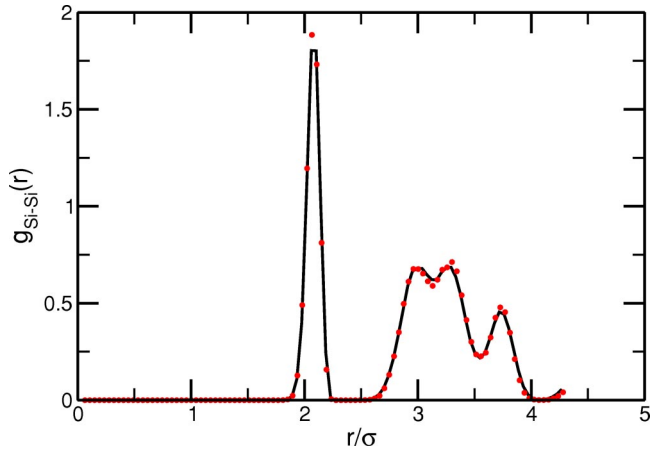

FIG. 9. Si-Si radial distribution functions of α and β quartz phases from the model. The solid line is for α quartz and the dots are for β quartz.

ate pressures, and coesite stable at the highest pressures studied. We note again that stishovite was not considered in this model due to the change in oxygen coordination about the silicon atoms under extremely high pressures,

In addition to the three crystalline phases, the current model finds a fluid phase that is in equilibrium with each solid phase. Figure 6 shows that slope of the melting line is relatively insensitive to different crystal phases, and that the model melts at a temperature range between $T^*=0.09$ and 0.10. The dashed lines in Figs. 6 and 8 denote our estimates of the fluid-solid equilibrium for states where we were unable to equilibrate the fluid phase to the extent necessary for a reliable estimate of the free energy. At lower temperatures we have estimated the fluid phase free energy using the ideal gas approximation. At these lower temperatures it is shown in Fig. 6 that cristobalite can be in equilibrium with a low density vapor-like (ideal gas) phase as well as with quartz. We now turn our attention to the nature of the fluid phase with which the solids are in equilibrium.

Experimental data suggest that the liquid (or glass-like phase) has a density lower than that of the crystalline phase. The one exception to this is β cristobalite, which is a few percent less dense[46] than the liquid. Figure 8 shows the computed density ($\rho\sigma^3$) versus temperature (kT/ϵ) phase diagram of the system. We can see that above moderate pressure quartz and coesite are in equilibrium with a fluid that is slightly less dense than the crystal phase. However, at lower pressures, it is shown that quartz and cristobalite are in equilibrium with a much lower density fluid state. This is not in agreement with experimental data on the fluid phase, which show that the fluid phase is only a few percent less dense than the solid in question. At very low densities, relative to close packed arrangements, a transition to an ideal gas state is shown for a wide range of temperatures. The phase behavior of the current work is similar to that of the PMW.[24] In the case of the PMW, estimation of the low temperature, low pressure solid-fluid equilibrium was aided by the use of a thermodynamic perturbation theory,[24,47–49] which is unavailable for the present model. The PMW shows a metastable liquid+vapor equilibrium that lies entirely inside the low density solid+fluid region of the phase diagram. It is possible that this behavior is present in the current model as well.

While the model is able to describe phases that differ by pressure, it does not appear to distinguish between the α and β phases of a given polymorph. The α and β phases of a polymorph have very similar crystal structures. The difference lies in that the β or high-temperature phase has a higher symmetry associated with its crystal structure. In the present model when all bonds are saturated, as they are at low temperatures, changing temperature does not significantly influence bonding or structure. To better understand the equilibrium structure of α and β phases in our model, we examined the Si-Si radial distribution function (Figs. 9 and 10). As simulations of α quartz are equilibrated, we see that the second, third, fourth, and fifth crystal peaks of the Si-Si radial distribution functions merge into two peaks at $r=3.0\sigma$ and $r=3.3\sigma$. This shows that α quartz equilibrates into a ''quartzlike'' structure, but does not have the symmetry associated with the perfect crystal. Similar behavior is observed with β quartz: as the simulation proceeds towards equilibrium, the crystal peaks in the radial distribution function again merge into two peaks at $r=3.0\sigma$ and $r=3.3\sigma$. Figure 9 gives a comparison of the $g_{\text{Si-Si}}(r)$ for both α (line) and β (dots)

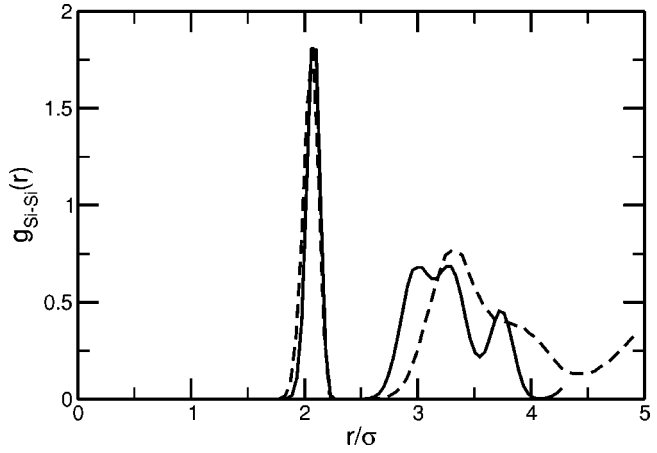

FIG. 10. Si-Si radial distribution function of quartz and cristobalite. The solid line gives the results for quartz and the dashed line for cristobalite.

Downloaded 29 Oct 2004 to 128.119.82.70. Redistribution subject to AIP license or copyright, see http://jcp.aip.org/jcp/copyright.jsp

quartz and indicates that both quartzes have the same ordering in our model. In Fig. 10, we also compare the $g_{\text{Si-Si}}(r)$ of quartz (solid line) and cristobalite (dashed line), showing that these phases have noticeably different equilibrium structures in the model.

IV. CONCLUSIONS

We have developed a simple molecular model of silica materials, which gives good qualitative agreement with experimental data on mechanical and phase equilibrium properties. The model consists of silicon, represented as a hard sphere with four bonding sites in tetrahedral locations on its surface and oxygen, represented as a hard sphere with two bonding sites fixed on its surface. Isobaric-isothermal and isochoric Monte Carlo simulations were applied to this model. Density, isotherms, bulk moduli, thermal expansion coefficients, three body angle distributions, and radial distribution functions were computed and found to be in good qualitative agreement with known experimental data. Free energy calculations were made to construct a phase diagram for the model. This represents one of the first instances where the phase behavior of an atomistic model of silica has been calculated (we are aware of only one other study of this type,[50] which was done recently using a modified BKS potential[17]).

The model clearly distinguishes among cristobalite, quartz, and coesite, showing both quartz-cristobalite and quartz-coesite phase coexistence lines. A fluid phase was also found to be in equilibrium with each of the three solid phases. At low pressures and densities, a low density gas phase was found to be the thermodynamically stable phase. The temperature-density phase behavior is similar to that of the primitive model of water.[24] We find that coesite is in equilibrium with a fluid that is a few percent less dense, while quartz and cristobalite are in equilibrium with a fluid phase that is much less dense than the respective crystal structures. Given the similarity with the PMW, it is possible that a metastable vapor+liquid region exists within the cristobalite+fluid phase region.

These results show that a simple model can capture the qualitative phase and mechanical equilibrium behavior of silica-based materials. This model allows relatively large systems to be simulated in a reasonable time, in contrast to other more sophisticated models of silica. With suitable generalizations of this model, to account for the type of silica species present in basic aqueous solutions, it may become feasible to simulate self-assembly of silica nanostructures with atomistic detail.

ACKNOWLEDGMENTS

This work was supported by the National Science Foundation through a Nanotechnology Interdisciplinary Research Team (NIRT) Grant No. CTS-0103010.

[1] *Handbook of Zeolite Science and Technology*, edited by S. M. Auerbach, K. A. Carrado, and P. K. Dutta (Dekker, New York, 2003).
[2] D. D. Kragten, J. M. Fedeyko, K. R. Sawant, J. D. Rimer, D. G. Vlachos, R. F. Lobo, and M. Tsapatsis, J. Phys. Chem. B **107**, 10006 (2003).
[3] J. D. Sherman, Proc. Natl. Acad. Sci. U.S.A. **96**, 3471 (1999).
[4] M. E. Davis and R. F. Lobo, Chem. Mater. **4**, 756 (1992).
[5] O. Velev, T. Jede, R. Lobo, and A. Lenhoff, Nature (London) **389**, 447 (1997).
[6] R. Schroden, M. Al-Daous, and A. Stein, Chem. Mater. **13**, 2945 (2001).
[7] P. S. J. Russell, T. A. Birks, J. C. Knight, R. F. Cregan, B. Mangan, and J. P. D. Sandro, Jpn. J. Appl. Phys. **37**, 45 (1998).
[8] J. Beck, J. C. Vartuli, W. H. Roth *et al.*, J. Am. Chem. Soc. **114**, 10834 (1992).
[9] V. Nikolakis, E. Kokkoli, M. Tirrell, M. Tsapatsis, and D. G. Vlachos, Chem. Mater. **12**, 845 (2000).
[10] S. Mintova and V. Valtchev, Microporous Mesoporous Mater. **55**, 171 (2002).
[11] C. E. A. Kirschhock, R. Ravishankar, L. V. Looveren, P. Jacobs, and J. A. Martens, J. Phys. Chem. B **103**, 4972 (1999).
[12] C. E. A. Kirschhock, R. Ravishankar, F. Verspeurt, P. J. Grobet, P. Jacobs, and J. A. Martens, J. Phys. Chem. B **103**, 4965 (1999).
[13] R. Ravishankar, C. E. A. Kirschhock, P. Knops-Gerrits *et al.*, J. Phys. Chem. B **103**, 4960 (1999).
[14] S. Tsuneyuki, M. Tsukada, H. Aoki, and Y. Matsui, Phys. Rev. Lett. **61**, 869 (1988).
[15] P. Vashishta, R. Kalia, and J. Rino, Phys. Rev. B **41**, 12197 (1990).
[16] B. Vessal, M. Leslie, and C. R. A. Catlow, Mol. Simul. **3**, 123 (1989).
[17] B. W. H. van Beest, G. J. Kramer, and R. A. van Santen, Phys. Rev. Lett. **64**, 1955 (1990).
[18] J. S. K. P. Schroder and J. Sauer, J. Phys. Chem. **100**, 11043 (1996).
[19] B. Vessal, M. Amini, D. Fincham, and C. Catlow, Philos. Mag. B **60**, 753 (1989).
[20] S. Chaplot and S. Sikka, Phys. Rev. B **61**, 11205 (2000).
[21] L. Haung and J. Kieffer, J. Phys. Chem. **118**, 1487 (2003).
[22] D. Ghonasgi and W. G. Chapman, Mol. Phys. **79**, 291 (1993).
[23] J. Kolafa and I. Nezbeda, Mol. Phys. **61**, 161 (1987).
[24] C. Vega and P. A. Monson, J. Chem. Phys. **109**, 9938 (1998).
[25] R. Wyckoff, *Crystal Structures* Vol. 2 (Interscience, New York, 1965).
[26] A. F. Wright and A. J. Leadbetter, Philos. Mag. A **31**, 1391 (1973).
[27] G. M. Clark, *Structure of Non-Molecular Solids* (Applied Science, London, 1972).
[28] R. C. Evans, *An Introduction to Crystal Chemistry*, 2nd ed. (Cambridge University Press, Cambridge, 1964).
[29] L. Levien and C. T. Prewitt, Am. Mineral. **96**, 324 (1981).
[30] C. Baerlocher, W. M. Meier, and D. H. Olson, *Atlas of Zeolite Framework Types*, 5th ed. (Elsevier, Amsterdam, 2001), http://www.iza-structure.org/databases
[31] M. Parrinello and A. Rahman, Phys. Rev. Lett. **45**, 1196 (1980).
[32] P. Najfabadi and S. Yip, Scr. Metall. **17**, 1199 (1983).
[33] S. Yashonath and C. N. R. Rao, Mol. Phys. **54**, 245 (1985).
[34] D. Frenkel and J. Ladd, J. Chem. Phys. **81**, 3188 (1984).
[35] C. Vega, E. P. A. Paras, and P. A. Monson, J. Chem. Phys. **96**, 9060 (1992).
[36] J. M. Polson, E. Trizac, S. Pronk, and D. Frenkel, J. Chem. Phys. **112**, 5339 (2000).
[37] C. Vega, E. P. A. Paras, and P. A. Monson, J. Chem. Phys. **97**, 8543 (1992).
[38] W. N. Shen and P. A. Monson, J. Chem. Phys. **103**, 9756 (1995).
[39] Q. Yan and J. J. dePablo, J. Chem. Phys. **111**, 9509 (1999).
[40] F. G. Wang and D. P. Landau, Phys. Rev. Lett. **86**, 2050 (2001).
[41] Q. Yan, R. Faller, and J. J. dePablo, J. Chem. Phys. **116**, 8745 (2002).
[42] M. S. Shell, P. G. Debenedetti, and A. Z. Panagiotopoulos, Phys. Rev. E **66**, 056703 (2002).
[43] J. J. Pluth, J. V. Smith, and J. Faber, Jr., J. Appl. Phys. **57**, 1045 (1985).
[44] L. Levien, C. T. Prewitt, and D. J. Weidner, Am. Mineral. **65**, 920 (1980).
[45] R. F. Pettifer, R. Dupree, I. Farnan, and U. Sternberg, J. Non-Cryst. Solids **106**, 408 (1988).
[46] C. A. Angell and H. Kanno, Science **193**, 1121 (1976).
[47] J. Kolafa and I. Nezbeda, Mol. Phys. **61**, 161 (1987).
[48] M. S. Wertheim, J. Stat. Phys. **35**, 19 (1984).
[49] M. S. Wertheim, J. Stat. Phys. **35**, 35 (1984).
[50] I. Saika-Voivod, F. Sciortino, T. Grande, and P. Poole, arXiv:cond-mat/0406192 (2004).
[51] V. Swamy, S. K. Saxena, B. Sundman, and J. Zhang, J. Geophys. Res. **99**, 11787 (1994).
[52] H. van Koninsveld, H. van Bekkum, and J. C. Jansen, Acta Crystallogr., Sect. B: Struct. Sci. **43**, 127 (1987).

Downloaded 29 Oct 2004 to 128.119.82.70. Redistribution subject to AIP license or copyright, see http://jcp.aip.org/jcp/copyright.jsp